ICAS-88-5.6.4

POST-BUCKLING BEHAVIOR OF LAMINATED COMPOSITE STIFFENERS AND STIFFENED PANELS UNDER CYCLIC LOADING.

Y. Frostig, G. Siton, A. Segal
Israel Aircraft Industries, Ben-Gurion Airport , Israel.

I. Sheinman, T. Weller
Technion - Israel Institute of Technology, Haifa, Israel.

Abstract

Results of an experimental and analytical study of the Post-Buckling of selected graphite-epoxy stiffeners subjected to static and cyclic axial compression loading are presented. Post-Buckling behavior and failure characteristics are described. Stiffeners sections include I and J shapes, commonly used in stiffened panels, with an attached 12 plies skin. Failure of all specimens, regardless of shape, was associated with delaminations in cap and cracks and fibres breakage in the attached skin. Analytical results from a non-linear stiffened panel analysis computer code correlated well with post-buckling test results. The analytical modelling necessary to predict accurately the response of the stiffener is described. The cyclic loading has a favorable effect on the failure loads compared with the specimens loaded statically.

1. Introduction

Metallic stiffened panels and shells are sometimes designed to buckle below design limit load. The degree of post-buckling depends on the type of structure and it is often limited due to non-structural considerations such as aerodynamic requirements, etc.. Wing and empennage covers are sometimes allowed to buckle below limit load. Fuselage panels, on the other hand, are usually designed to sustain stresses of three to four times those corresponding to initial buckling. Collapse of such structures is characterized by a ductile failure, e.g. large deformations. This form of collapse is due to the plastic capability of the material.

Design of more efficient composite structures can be achieved if more data on post-buckling behavior and strength will exist. Significant weight savings are projected if composite structures can be utilized in the post-buckling region. Presently, graphite-epoxy structures are limited to non-buckling load levels, due to lack of experimental data and analytical methodology. In fuselage structures compression members account for a significant fraction of the total structural weight. The ability to increase the load carrying capacity of these members by operating them in the post-buckling region offers even greater weight savings than heretofore possible.

Failure of compressed stiffened composite panels is usually controlled by the carrying capacity of its stiffeners. A thorough understanding of the stiffener behavior under static and cyclic compressive loads will lead to better predictions of the panel behavior, especially in the post buckling region, and failure characteristics. Failure predictions are usually based on equivalent section concept, e.g. a typical section consisting of stiffener and skin. The attached skin width equals to the typical "effective width" in the panel, see [16].

In view of these considerations an investigation of the initial and local buckling, post buckling and crippling behavior of Graphite-Epoxy stiffeners was conducted. Among the important objectives of the study were; 1) to evaluate the feasibility of utilizing the post-buckling strength of the stiffener under static and cyclic compressive loadings, 2) to allow prediction of the behavior and failure characteristics of a complex structure, like stiffened panels based on its constituent behavior.

A large number of publications dealing with post-buckling of metallic panels under compression and shear loads appear in the literature, see for example [1] and [2]. An immense number of research works have been performed regarding the buckling behavior of metallic plates. During the last decades the classical buckling problem was extended, to some extent, to anisotropic plates, see Ashton [3-6], Agrawal [7], Kudva [8] on shear panels, Starnes [9-10] and Chia [11]. The publications on stiffened composite panels are limited, Leissa [12] cited a few references using analytical procedures for prediction of the post-buckling behavior. A design procedure for stiffened panels appears on refs. [13-14]. Starnes et al., refs. [9-10], tested a stiffened panel under static compressive load. The experimental results related well with the analytical ones, using the STAGSS-C1

Copyright © 1988 by ICAS and AIAA. All rights reserved.

code [9]. The failure pattern reported, for all the tested panels, started at the interface between the skin and the stiffener, causing separation of the stiffener from the skin. Publications on fatigue effects are rarely found in the open literature and among the few we can cite are refs. [15-16]. Renieri et al., [17], dealt with the post-buckling of thin-walled compression members under static compressive loads.

The paper describes the results of a study consisting of tests and analysis of thin-walled stiffeners with an attached skin. The experimental part includes static as well as a cyclic compression, at loads levels in post-buckling range. The analytical part includes results from a code, named "PBCOMP". The program predicts the post-buckling behavior of stiffened panels as well as thin-walled stiffeners and models the structure as separate plates connected through compatibility and continuity conditions. Results include post-buckling behavior at various parts of the structure as well as overall behavior, while allowing coupling between local buckling to overall behavior. The analytical results were in good agreement with the experimental ones, as demonstrated for a typical test specimen.

The experimental part is discussed in next, followed by the analytical results and concluded with recommendations.

2. Experimental Program

The experimental part included 11 specimens consisting of I and J shaped sections, see fig. 1 . Each group consisted of three "long" specimens, 750 mm and three "short" ones ,250 mm in length. The "long" ones were used to define local and overall buckling under static and cyclic compressive loads, while the other group defined the crippling load capacity of the stiffeners. The first group ("long") sections included stiffener section and an attached skin of 90 mm width. The additional skin allowed modelling the stiffener behavior within a stiffened panel with the aid of "effective width" concept, see [16].

The first of the "long" specimens was statically loaded to failure and the others were cycled to 250k cycles. The cyclic loading part details, such as load levels and number of cycles per block are summarized in tables 1 and 2. Dimensions and layups are shown on fig. 1 for the various configurations.

The eleven specimens were designed and manufactured by Israel Aircraft Industries (I.A.I.) and were tested at the Structures Laboratory of the Aeronautical Department at Technion. The specimens were fabricated of AS4/3502, graphite-epoxy tape material. This material is 350 F cure type and is commonly used in composite aircraft structures. The manufacturing

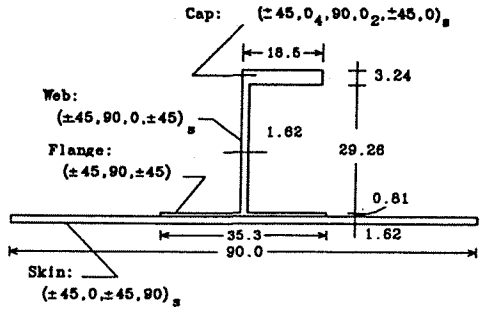

b) J – Stiffener

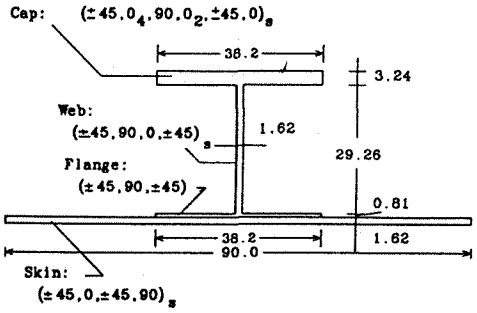

a) I – Stiffener

Figure 1: Geometrical and stacking sequence of typical I and J shape stiffeners.

process consisted of one curing cycle with the stiffener integrally laid into the skin and cocured with it.

All specimens were manufactured in one step, by fabricating a large panel and cutting it to the proper dimensions. The "long" ones included a skin of 90 mm in width, while the crippling specimens included a skin equal to lower flange width. The three "short" specimens were produced by cutting a "long" one to three equal parts. This procedure allowed all specimens to be manufactured under the same conditions.

The stiffener skin separation failure mode, reported in ref. [9-10] was prevented by overlapping of the two upper plies of the skin on the stiffeners lower flange. The maximum strains level involved in the skin-flange attaching zone were around the 1.0%.

Following curing the specimens were ultrasonically inspected to establish specimen quality. No defects were detected. The ends of each specimen were potted in an epoxy-resin mixed with chopped glass fibres encased in a U shaped aluminum channel. The loaded ends were machined flat and parallel to permit uniform end-shortening compressive load. The specimens were painted white on both sides to enhance the Moire fringes pattern and brooming of black graphite fibres.

2.1 Test Results

The testing program consisted of 11 specimens, two groups of three "long" specimens, I and J shaped respectively. The specimens for crippling included three I shaped and two J shape types. The first specimen in the "long" group items was used as a reference, to determine initial buckling and failure load levels. The other two were cycled at load levels defined by the reference item. Details of the cycling program appear on tables 1 and 2 for I and J stiffeners, respectively. A static residual strength test was conducted after completion of the cyclic loading program.

The "short" specimens were tested for crippling strength only. Results ,summarized in table 3, included failure loads and initial buckling loads based on end-shortening versus applied load diagrams.

The specimens were instrumented by strain-gages bonded back to back at at the following locations: skin edges, intersection points of ends of flange and attached skin, center of web and cap edges. In J-shaped stiffeners also at web-cap intersection points. Out of plane and horizontal deflections of stiffeners caps, were monitored with the aid of a LVDT apparatus at the cap-web intersection. Experimental results for each specimen included average and bending (non-dimensional curvature) strains, end-shortening and displacements versus the applied load. The I shape stiffener are discussed next, followed by the J group.

2.1.1 I-Stiffeners

The reference specimen, I1 was monitored by strain-gages at two sections. The first one, section B-B, 100 mm from the lower loaded end and the second one, section A-A, at the crest of a halfwave. Uniformity and eccentricity of exerted load was monitored by the strain-gages located at section B-B. The buckled mode shapes were visualized with the aid of a moire shadow-fringe technic.

The stiffener was statically loaded up to failure to define initial buckling and failure load levels. No initial curvature was observed. Formation of buckling halfwaves, at midspan, started at 4400 kg, and was fully formed at 6000 kg., see fig. 2. Failure occurred at 8700 kg., while prediction based on equivalent gross section was 9000 kg., see fig. 3. Collapse followed the known trends of column-buckling, associated with delaminations in the cap and cracks and fibres breakage in the attached skin, cocncentrated at mid-span. No separation of skin from stiffener was detected. Initial instability load, based on average strains versus total loads curves, at skin edges, yielded 5300 kg (see table 1 for more details). Initial buckling based on

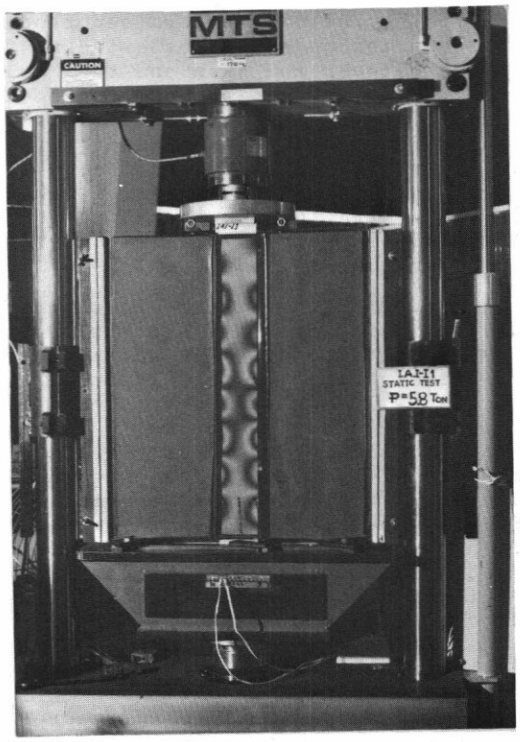

Figure 2: Buckling mode shapes, I1.

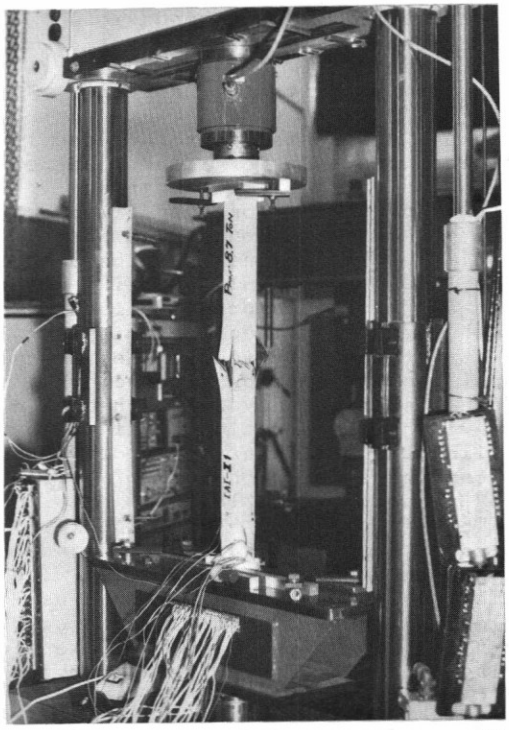

Figure 3: Failure pattern, specimen I1.

end-shortening curves yielded a different value, listed on table 1.

The second and the third specimens were cycled to 250k cycles at load levels around the initial buckling load level. Strain-gages pattern was changed and

concentrated at the crest of buckled halfwave to allow more measurements informations on the behavior.

Results are presented and discussed for I2 specimen only, since the third one, I3, behavior was nearly identical, except for failure load. The specimen ,I2, was first statically loaded to 5500 kg. and then lowered to 5000 kg. for cyclic loading. After 170 cycles noises were heard and delamination at the lower end of the specimen was detected. The damage was probably due to eccentricity of exerted load and irregularities of specimen end resting on the aluminum U channel. The specimen was repaired and shortened to 680 mm, after being ultrasonically inspected for additional damage. No additional debondings or delaminations were detected.

The specimen was statically reloaded and then cycled, see table 1 for details. Completion of the cyclic loading program was followed by a residual strength test. Buckling mode shapes pattern is shown on fig. 4. Excessive deformations were observed prior to failure, see fig. 5. Collapse occurred at 9400 kg, initiated by cracks in the attached skin followed by delaminations in the cap. Failure pattern was identical with that of the third specimen, I3, but at a lower load, see fig. 11. The measured strains were around 0.8% to 0.9%. Prediction based on gross section and reduced length yielded a failure load of 11000 kg..

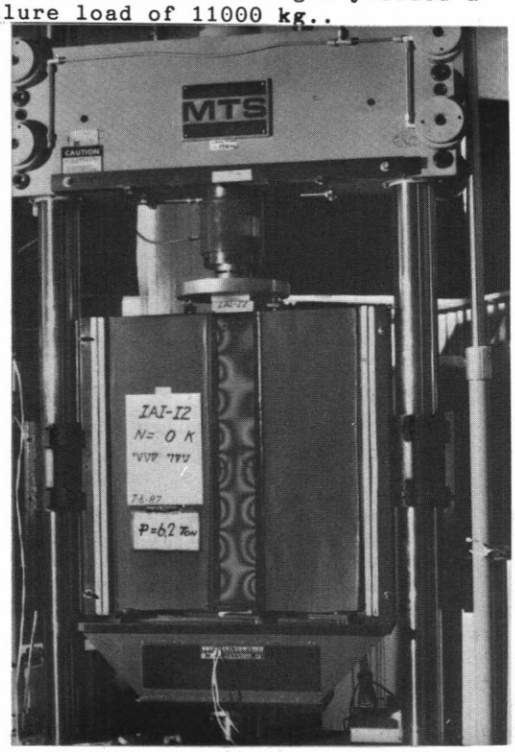

Figure 4: Buckling modes shapes, I2, Length=680mm.

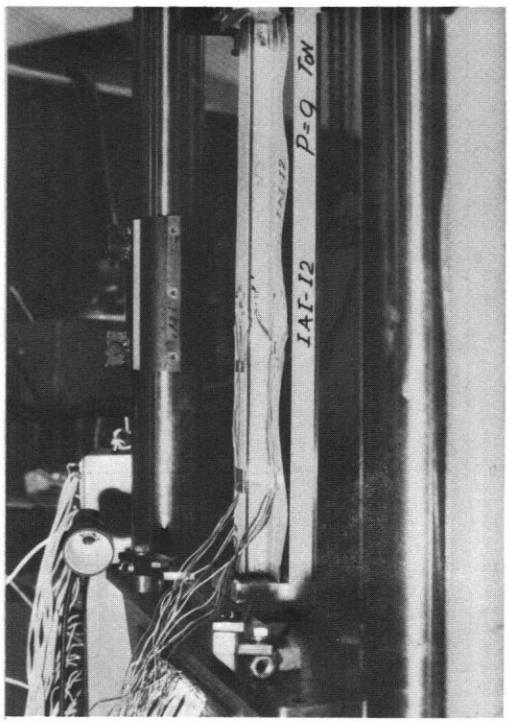

Figure 5: Skin edge deflections, I2, at P=9000 kg., prior to failure.

Graphical representations of the behavior are shown on the following figures. Total force versus average strains at attached skin and flange, locations 1 to 4 appear on fig. 6. The behavior changed trends at initial buckling load level. The attached skin behaved as a part of the gross section, below initial buckling load level, while above it, its axial rigidity deteriorated, or in other words, the gross section didn't preserve its shape. Loss of stability at locations 4 and 7 was associated with lower average strains and with very large bending strains, see fig. 7. Locations at skin-flange intersection points retained their axial rigidity, thus reduction in compressive strains at skin edges was accompanied with an increase of compressive strains at these intersection points. The curvatures or bending strains on one edge of the skin were opposite to the other edge, see fig. 7. Location 4 was subjected to larger deformations compared with the other point, location 7, near failure load.

One of the questions associated with the study looked in the coupling effects of the local buckling of the various parts of the stiffener with the overall behavior. Web average strains versus total load appear in fig. 8. No loss of rigidity or local buckling resistance was observed. The strains at cap edges, locations 1 and 2, were antisymmetrical, as shown on fig. 9. Strains at location 1 decrease while those at other edge increased, namely the cap bent horizontally, in its own plane. Bending

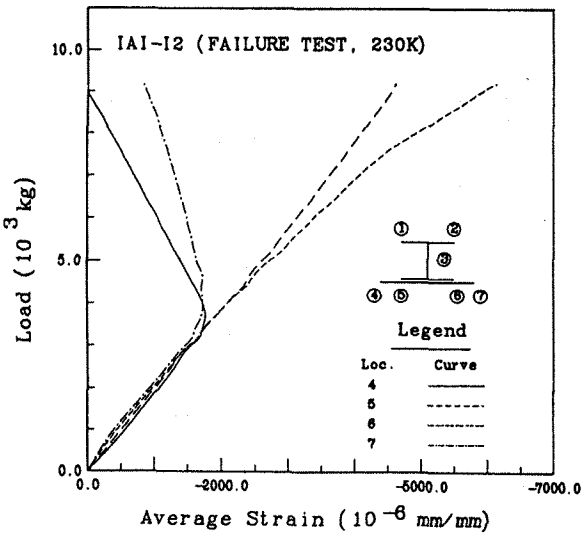

Figure 6: Load versus longitudinal average strains, I2, at attached skin edges and flange, at mid-span, after 230k cycles, Length=680mm.

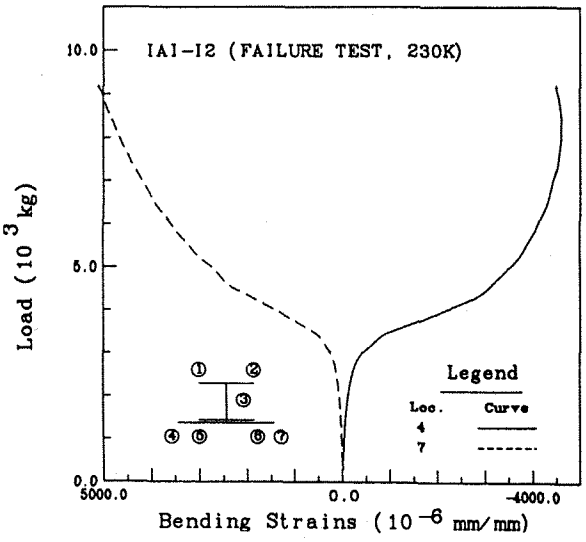

Figure 7: Longitudinal Bending strains (curvatures), I2, at skin edges, after 230k cycles, Length=680mm.

strains (curvatures) of this part, see fig. 10, resemble the known trends of column-buckling with imperfections, leading to the conclusion that the cap actually buckled prior to overall failure of the stiffener. This phenomenon indicated that as load was increased buckling of cap was initiated leading to a premature collapse of the overall section. Cyclic loadings neither affected the initial buckling loads nor the overall behavior. This is different then was observed in the stiffened panel tests, ref. [16].

Another question which the study attempted to answer was wether an analysis

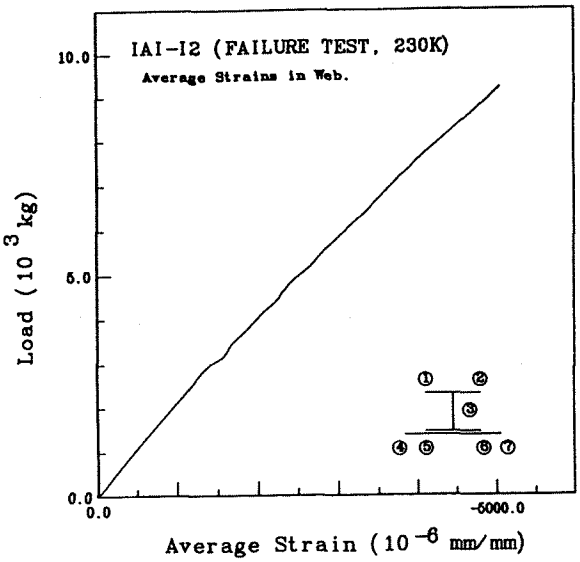

Figure 8: Longitudinal average strains, I2, at center of web, at mid-span, after 230k cycles, Length=680 mm.

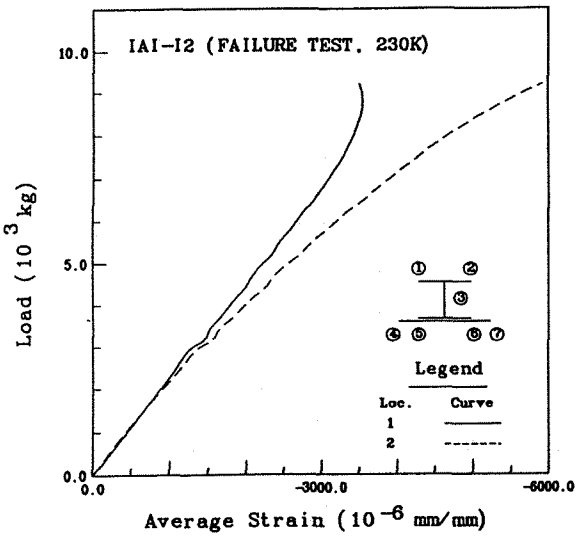

Figure 9: Longitudinal average strains, at cap edges, I2, at mid-span. after 230k cycles, Length=680mm

based on an undeformed section (beam analysis) was correct and justified. A beam analysis was justified as long as initial buckling didn't occur, while above it the gross section shape was not preserved. An analysis based on the stiffener section alone was recommended for loads above initial buckling load level. The strains distribution revealed that above initial buckling load some eccentricity was induced, either due to changes in boundary conditions at initial buckling load level or as a result of different imperfections in the two sides of the skin. Cyclic loading effects on the distribution were minor and insignificant.

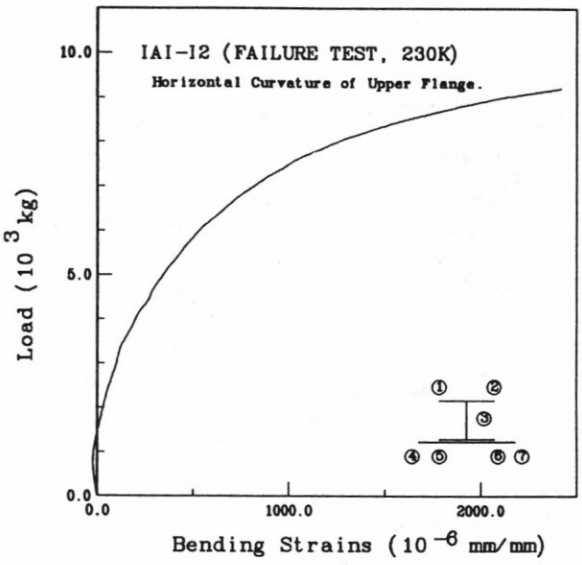

Figure 10: Cap horizontal curvature (bending strains), I2, at midspan, after 230k cycles, Length=680 mm.

The third specimen, I3, behavior was nearly identical to that of the second one. The same kind of damage, described above for I2, was observed at the beginning of the cyclic loading program. This time the specimen was loaded without any eccentricity, leading to the conclusion that the irregularities at the ends of the specimen, embedded in the potting, were the cause. The specimen was shortened and repaired as in the previous case. Details on load levels, cycles and initial buckling level appear in table 1. Collapse occurred at 10200 kg, see fig. 11, lower than the predicted one but higher compared with the second specimen failure load. This time failure was initiated by delaminations in cap and followed by cracks in skin.

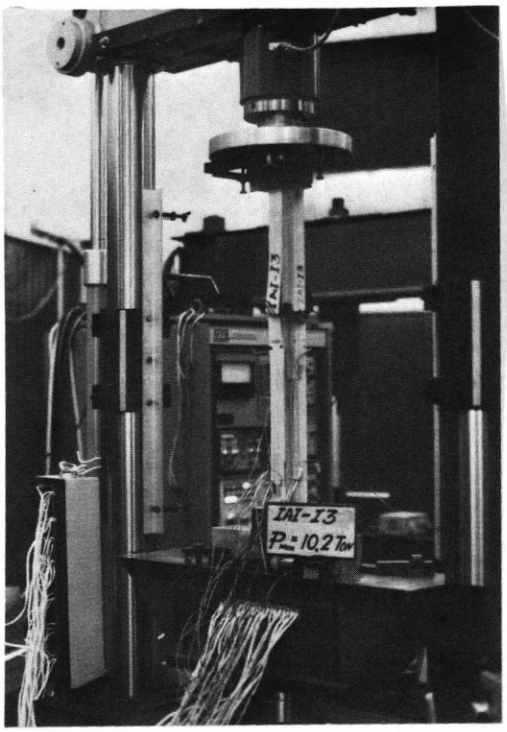

Figure 11: Failure pattern, I3, at P=10200 kg., Length=680 mm.

Crippling strength capacity was determined by testing the "short" specimens to failure. Strains were monitored at midspan only using strain-gages at center of each part of the stiffener.Irregularities at loaded ends affected the behavior causing premature collapse thus leading to a large scatter in the results, see table 3. Failure was always associated with cracks at lower ends at the flanges, see fig. 12.

Specimen	Cyclic Loading Range (kg)	Total Number of Cycles	Initial Buckling		Failure Load (kg)
			Load (kg)	Strains**	
I1	Static	-	4250 4350	2082(7) 1976(4)	8700
I2*	5000- 6000	230000	3640 3800	1773(4) 1732(7)	9400
I3*	5000- 6000	240000	3870 3510	1670(4) 1732(7)	10200

* Specimen was damaged at lower end at the beginning of cyclic program.

** Number in paranthesis are S.G's locations, see fig 6. Strains were measured in micro-strains, 10e-6 mm/mm.

Table 1 Summary of "long" I stiffeners, strains, buckling and failure loads.

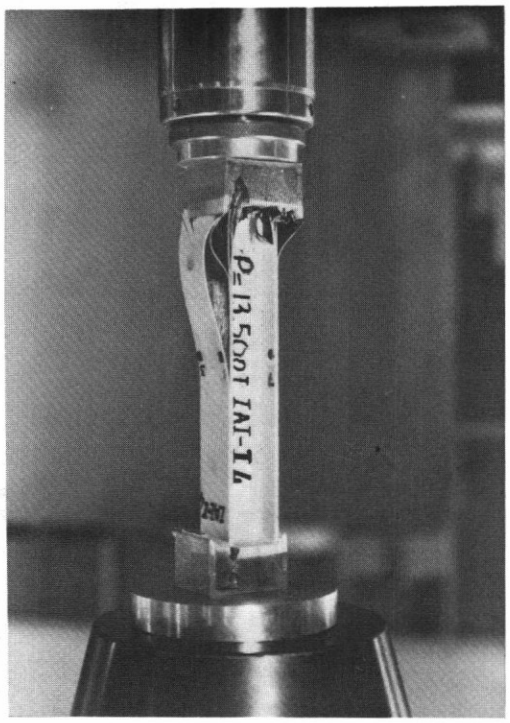

Figure 12: Collapse of crippling specimen, I4.

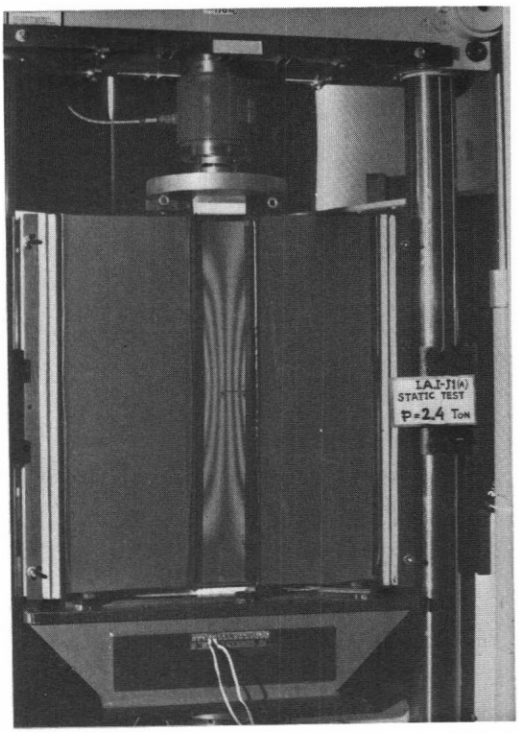

Figure 13: Buckling mode shapes, J1.

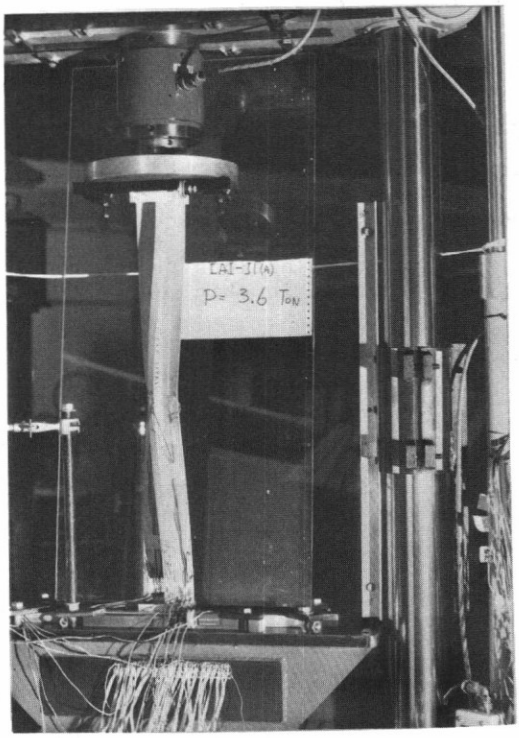

Figure 14: Stiffener deflections, J1, at P=3600 kg., prior to failure.

2.1.2 J-stiffeners

The first specimen, J1, was used as a reference item. The specimen was monitored by strain-gages, similar to I1 specimen pattern. The initial buckling and failure load levels were determined by loading the specimen to failure. No initial curvature was observed. Buckling mode shapes formation started at 2200 kg and was fully formed at 2600 kg, see fig. 13. The buckling mode shapes were different compared with the I stiffener ones, only one longitudinal wave was observed. Each edge of the skin was displaced opposite to the other, yielding the pattern shown on fig. 13. Stiffener deformations, prior to failure, were large, as shown on fig. 14. Failure occurred at 3875 kg, associated with delaminations in the cap and cracks and fibres breakage in the skin, at mid-span, see fig. 15. No separation of skin from stiffener was detected, although strain level at failure were around 0.9%

The second specimen, J2, was the same as the first one, but instrumented differently, similar to the I2 strain-gages pattern. The specimen was tested under cyclic compression, to 250k cycles. Testing program details are summarized on table 2. The buckling mode shapes were the same as for J1, but at a lower level, see fig. 13. Residual strength test followed completion of the cyclic loading program, yielding a failure load of 4450 kg, about 20% higher than the reference failure load. Failure pattern was nearly the same as that of the first one, J1, see fig. 16.

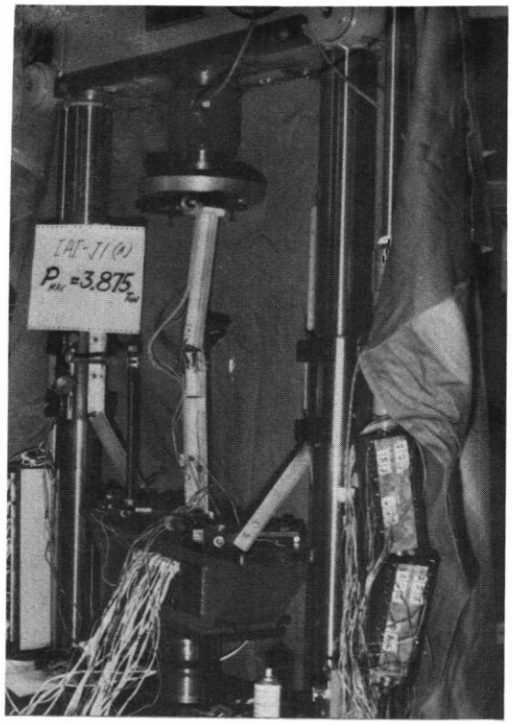

Figure 15: Failure pattern, J1 at P=3875 kg.

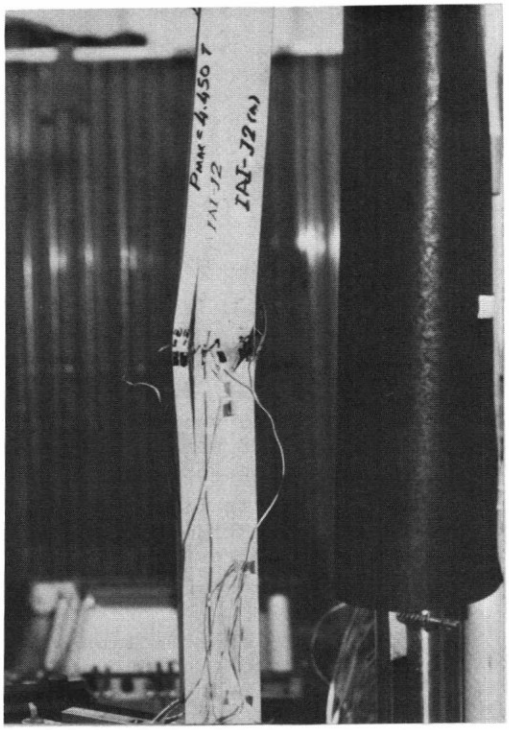

Figure 16: Failure pattern at P=4450 kg., J2.

Graphical presentations of the local and overall behavior are described in the following figures. Average and bending strains of upper flange and attached skin, at locations 1 to 4, are described on figs. 17 and 18. Loss of axial rigidity at locations 1 and 4 was observed at initial buckling load level, see fig. 17, and was expressed by reduction in the average compressive strains. The reduction in strains at skin edges was associated with an increase in compressive strains at locations 2 and 3. The gross section shape was preserved below initial buckling load while above it the section deformed, thus if beam analysis is used, the gross sections should be considered for loads below initial buckling level and stiffener section alone for loads above it. The behavior didn't follow that of an unsymmetrical section above initial buckling load level. The compression-tension strains in the lower flange showed that the cap buckled prior to collapse of the stiffener. In view of the above results, an analysis, modelling the

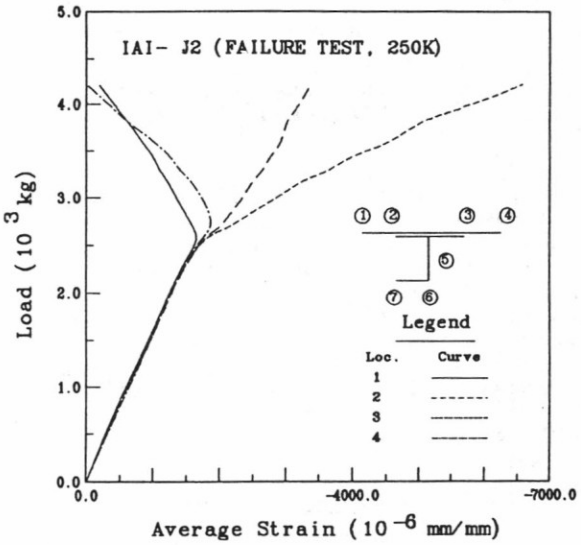

Figure 17: Longitudinal average strains at skin and flange edges, J2, at mid-span, after 250k cycles.

structure as made of separated plates connected through equilibrium and compatibility conditions, was recommended.

The unsymmetrical behavior of the stiffener is demonstrated through the bending strains of skin edges, locations 1 and 4, see fig. 18. Location 4 was displaced much more then the other edge, location 1, due to the non-symmetrical bending of the section. Local buckling or bending of various parts of the stiffeners appear on figs. 19 to 22. An abrupt change in the behavior of the various part of the stiffener was observed at initial buckling load level. Horizontal bending of the upper flange started at initial buckling level only, see fig. 19. Average and bending strains of the web are described on figs. 20 and 21 respectively. At 2440 kg the web axial rigidity was lost temporarily and was regained at 3000 kg, see fig. 20. The abrupt change was due to the initial buckling related to the change

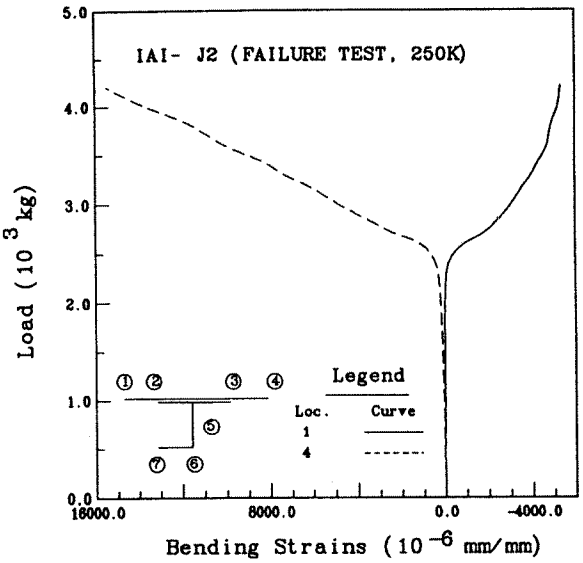

Figure 18: Bending strains (curvatures), at skin edges, J2, after 250k cycles.

in behavior of locations 1 and 4. Web vertical bending strains (curvatures) followed the trends of column-buckling as load was increased towards failure, see fig. 21. Cap horizontal bending is described on fig. 22. At 3530 kg, small changes in loads were associated with the decrease of average compressive strain and an excessive increase in the bending strains, leading to the conclusion that buckling of this part occurred.

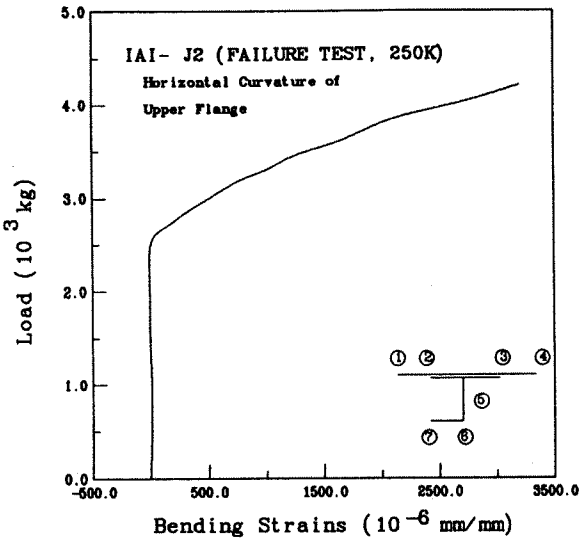

Figure 19: Horizontal bending strains, J2, at flange attached to skin, at midspan, after 250k cycles.

Cyclic loadings program didn't affect the local or overall buckling behavior, while failure load level was increased in about 20% compared with that of the reference specimen.

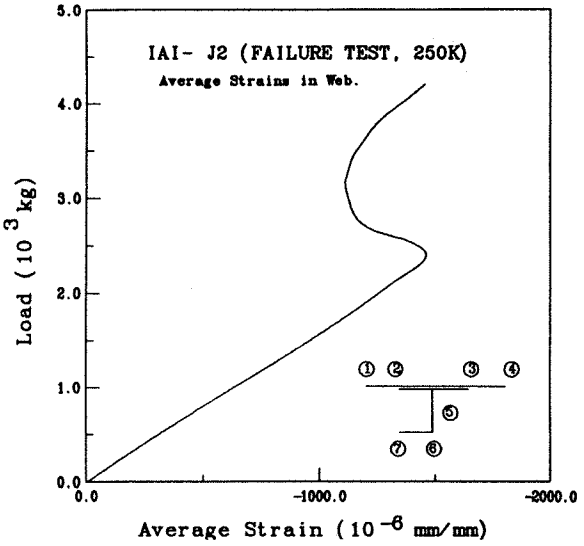

Figure 20: Longitudinal average strains, J2, at web center, after 250k cycles.

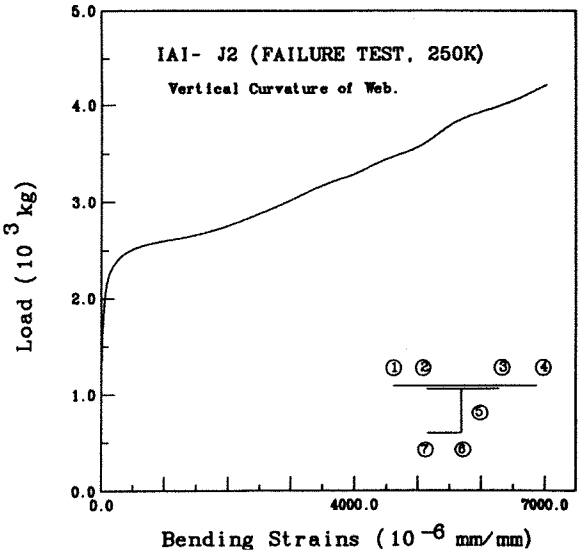

Figure 21: Vertical curvatures (bending strains) of web, J2, at mid-span, after 250k cycles.

Analytical results using the in house developed code, "PBCOMP", compared well with the experimental results of specimen J2. Details and discussions appear in next chapter.

Specimen J3 cap construction was different and had more contineous plies from web to cap compared with the previous ones. Some differences in behavior were observed compared with that of the previous specimens. Initial buckling, see fig. 23, using locations 4 was distinct while with location 1 the exact load level was blurred, probably due to large imperfections. Buckling mode shapes were nearly identical with those of the previous one, J2. Web behavior was

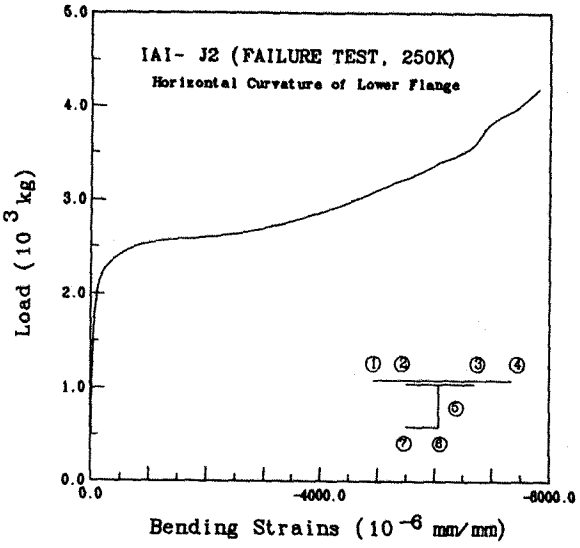

Figure 22: Cap horizontal curvature (bending strains), J2, at midspan, after 250k cycles.

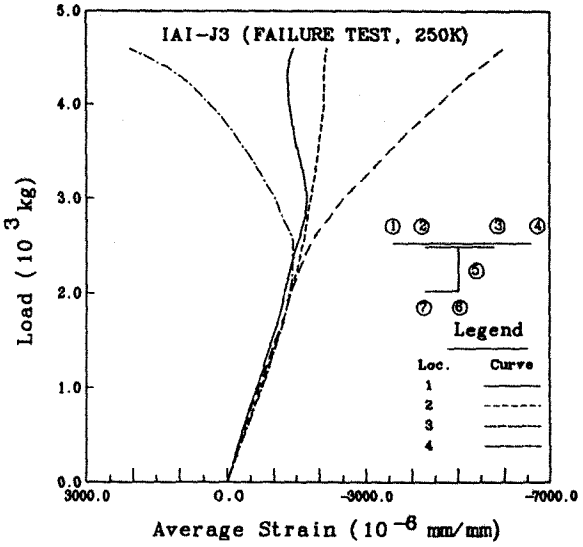

Figure 23: Longitudinal average strains, J3, at midspan, after 250k cycles.

different, see fig. 24, and the loss of axial rigidity reported earlier for the previous specimen didn't occur, probably as a result of local buckling of the web.

Failure occurred at 4800 kg, which is about 30% present above reference failure load and 10% above that of the second specimen. Collapse was associated with cap delaminations and cracks in the skin, at mid-span, see fig. 25.

Only two J-shaped specimens were tested for crippling strength, yielding failure loads of 8000 kg for J4 and 7500 kg for J5 specimens. More details appear on table 3. Failure mode was associated with delaminations in the flanges and cracks in the web, see fig. 26. Maximum measured average strains around failure were in the range of 0.8% to 1.1%.

Prediction of the failure of a stiffened composite panel using the results from this study correlated well with test results reported in ref. [16].

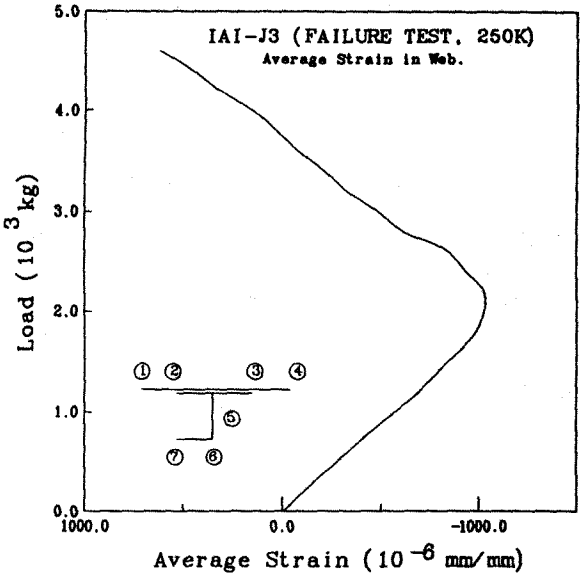

Figure 24: Average strains at web center, J3, at mid-span, after 250k cycles.

Specimen	Cyclic Loading Range (kg)	Total Number of Cycles	Initial Buckling		Failure Load (kg)
			Load (kg)	Strains*	
J1	Static	-	2760 2290	1758(1) 1758(4)	3875
J2	1900-2500	250000	2590 2750	1638(4) 1732(1)	4450
J3	1800-2450	250000	2400 3000	1429(4) 1743(1)	4800

* Number in paranthesis are S.G's locations, see fig 17. Strains were measured in micro-strains, 10e-6 mm/mm.

Table 2 Summary of "long" J stiffeners, strains, buckling and failure loads.

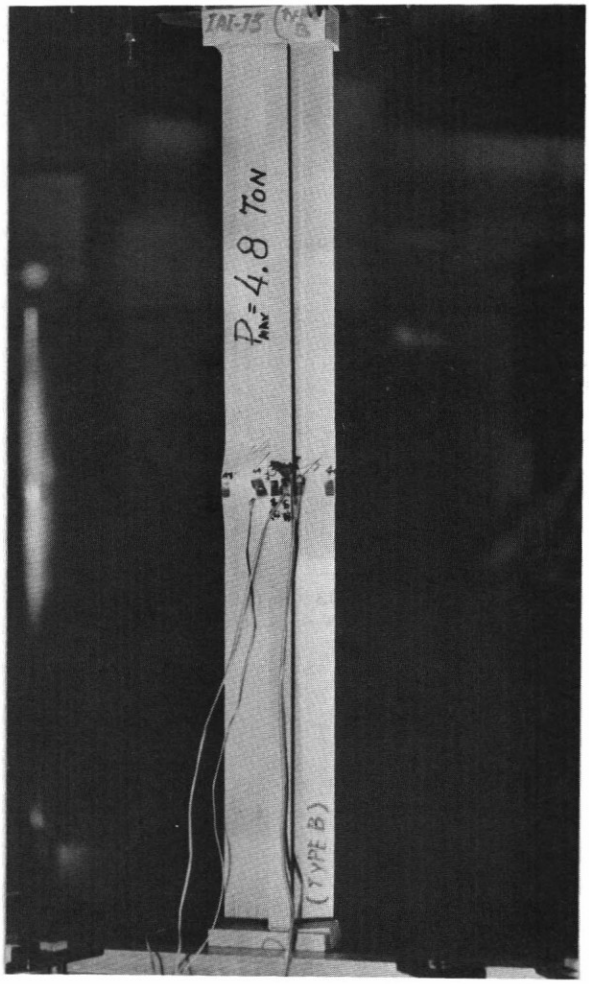

Figure 25: Failure pattern, J3, at P=4800 kg.

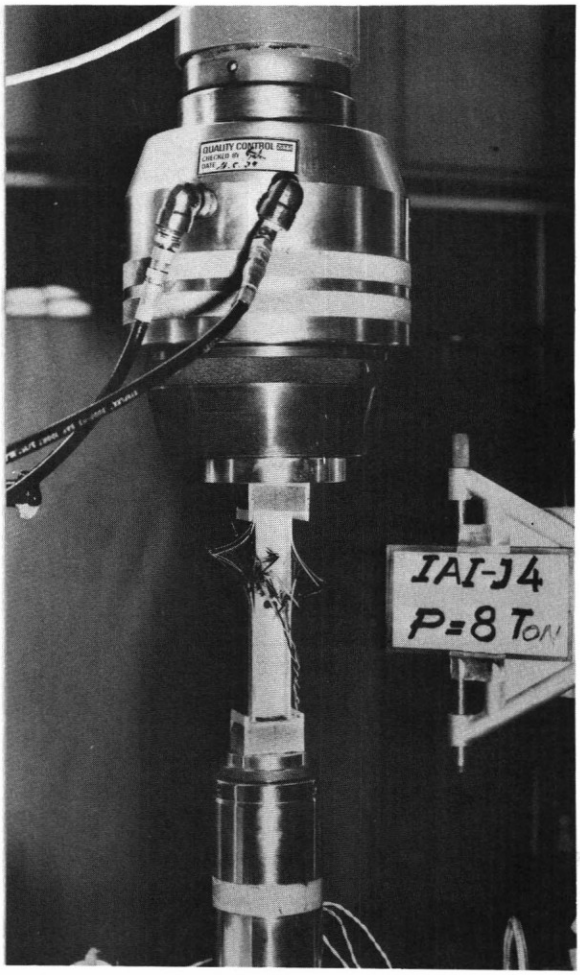

Figure 26: Collapse of crippling specimen, J4.

Specimen	Failure *		Local buckling	
	Load (kg)	Max. Strain	Load (kg)	End-short. (mm)
I4	13500	9775	6300	1.6
I5	9500	9075	6500	1.92
I6	11750	10547	7000	1.92
J4	8000	8743	4000	1.56
J5	7500	8202	4250	1.65

* Strains are measured in micr-strains (ms), 10E-6 mm/mm.

Table 3 Crippling strength of "short" I and J stiffeners.

3. Analysis

A J stiffener buckling behavior was investigated analytically using an in-house developed program, PBCOMP, see ref. [18,19], using J2 specimen data.

The program models any flat longitudinally stiffened panel as made of separated plates strips, transversely connected through equilibrium and compatibility conditions. Behavior equations are non-linear and allow large displacements with small rotations. The non-linear equations are described in terms of the unknowns, Airy stress function and the lateral deflection. The equations are replaced by resolving the two unknown functions into eigenfunctions in the longitudinal direction and applying a finite differences scheme in the transverse one. Imperfections assume the form of the eigenfunctions longitudinally, and constant or a sine function in the other direction. Galerkin procedure is used with view to minimum error in the truncation process. Then by means of Newton's method, the non-linear set of equations is converted into a linear sequence. The use of plate strips allows local buckling as well as overall responses.

The code, PBCOMP, is capable of dealing with arbitrary boundary conditions, longitudinally as well as transverse, loaded by combined inplane loads as well as longitudinal uniform end-shortening loading pattern. Laminates layup can be arbitrary and is not limited to special constructions. Stiffener geometry can be of any thin-walled shape. Output may includes internal stress resultants, bending moments, deformations, end-shortening as well as curvatures (bending strains) and average strains.

The analytical model for specimen J2 assumed that the various plates, were clamped at the longitudinal ends and free on the transverse sides, loaded at the longitudinal ends only. The equivalent uniform end-shortening loading distribution was defined by redistributing the total applied load according to the elastic axial rigidity of each plate strip, assumed to be uniform within strip width, and unchanged during loading sequence.

Comparison of analytical results with the experimental ones are shown on figs. 27 to 31. Locations 1 to 4 average and bending strains comparisons appear on fig. 27 and 28 respectively. The various results correlated well as long as initial buckling load level was not reached. As load was increased the analytical results had the same trends but with larger values. End-shortening versus the total load experimental and analytical results are described on fig. 29. A discrepancy between the results occurred above initial buckling load level. Analytical vertical and horizontal deformations at web flange intersection point are described on figs

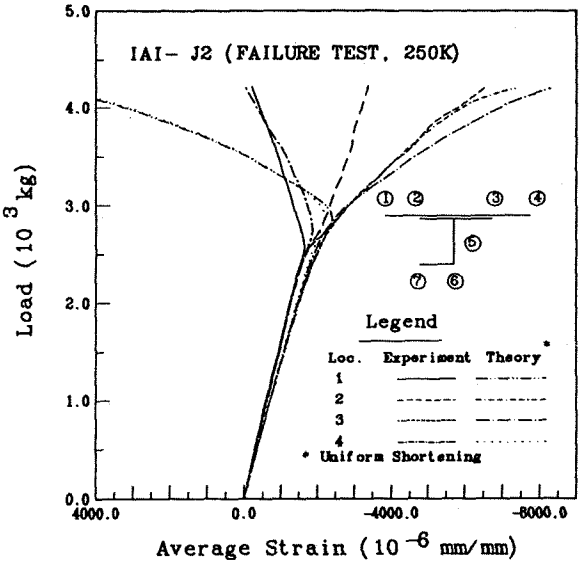

Figure 27: Longitudinal average strains, analytical and experimental results, J2, at midspan.

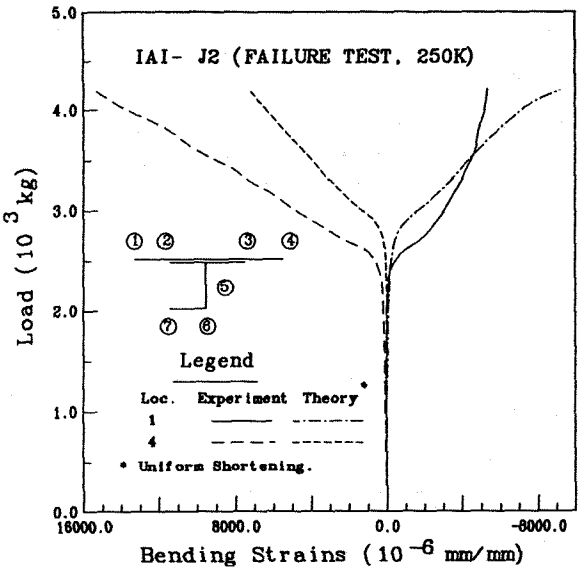

Figure 28: Analytical and experimental bending strains, J2, at skin edges.

30 and 31 respectively and compared well with the experimental ones. The experimental results were limited to 2800 kg. only, due to excessive deformations at higher loads.

The discrepancy in the results occurred in the non-linear range only. The analytical model was loaded by a constant distribution, based on axial rigidities, which was unchanged during the loading sequence. This distribution was correct as long as each plate maintained its axial rigidity. Above initial buckling load level, the attached skin lost its rigidity thus yielding a different load distribution, where the loads previously carried by these parts were transferred to

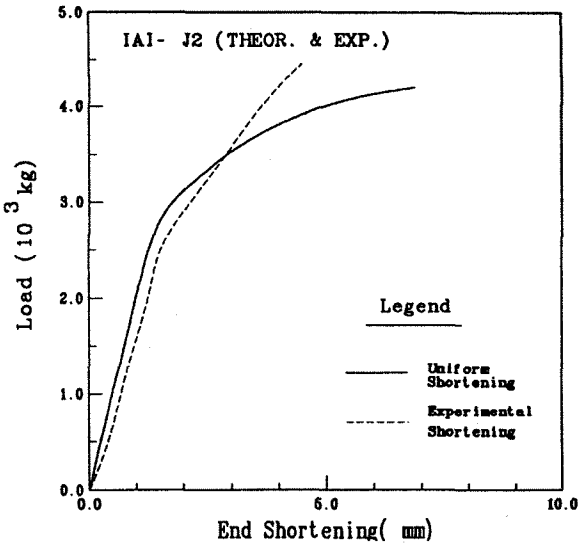

Figure 29: End-shortening versus total load, analytical and experimental results, J2.

the stiffener parts of the section. This change in loading was associated with smaller deformations since the majority of the load was carried by stiffer parts. In the analytical model, the deformations were larger compared with the experimental ones, since the load distribution was unchanged during the loading sequence .

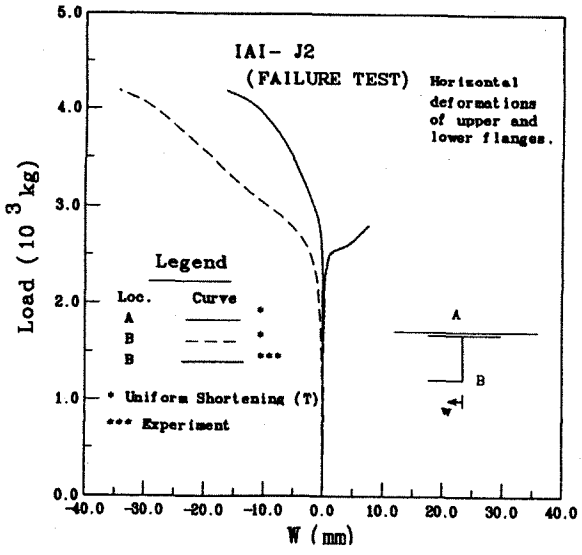

Figure 30: Horizontal deflection of J2 cap, analytical and experimental results.

4. Conclusions

An experimental and analytical investigation was conducted to study the buckling and post-buckling behavior of selected graphite-epoxy stiffeners loaded in axial compression. I and J shaped stiffeners with an attached skin, 90 mm wide, were examined.

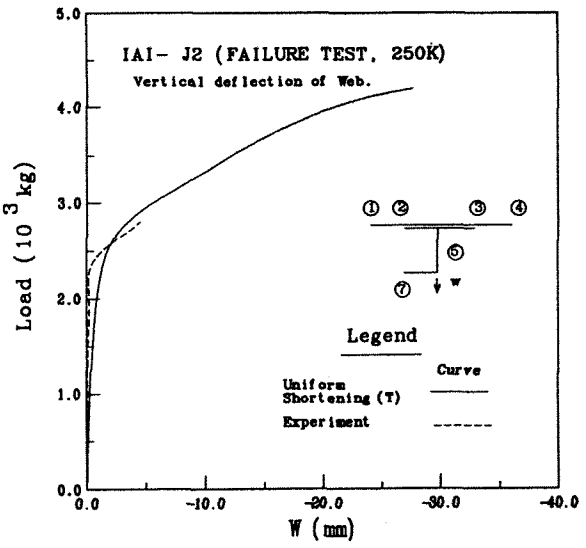

Figure 31: Out of plane deflection at web cap intersection point, J2, analytical and experimental results, at midspan.

The overall behavior was usually associated with initial buckling of the attached skin and beam-column buckling of the stiffener section only. The behavior of the various parts of the stiffener was abruptly changed as load passed the initial buckling level.

Predictions of failure loads of stiffened panels based on typical stiffener section including an attached "effective width " skin proved to be satisfactory, regardless of section shapes. Cyclic type loading had favorable effects on the failure loads, while minor changes were observed at initial buckling load levels. The cycled specimen failure loads were always higher compared with that of the statically loaded reference specimens.

The J stiffener with more continuous plies from web to cap, specimen J3, had a failure load of about 10% higher compared to sections with less continuous plies. Thus small changes in design without affecting weight can improve performance.

Failure pattern always included delaminations in cap and cracks and fibres breakage at attached skin. No separation of stiffener from skin was observed although strains level, at flange skin intersection points was between 0.8% to 1.0%.

Analytical predictions based on gross section, including attached skin were within engineering accuracy, provided that principal moments of inertia were used. In this method the coupling effects of local buckling on the overall behavior were neglected. Section shape was not preserved as load approach failure level, thus an analysis using PBCOMP, which allows distortion of the cross section is recommended.

Two typical shapes of stiffener were

examined, I and J , since they are often used in the design of stiffened panels. The I shaped stiffener weighed 20% more compared with the J type, but its carrying load capacity was 100% and more compared with the other group. The overall behavior was associated with smaller deformations and proved to be tougher compared ,with the other group.

Analytical results based on PBCOMP, using the tested specimen for data, were in good agreement with the experimental ones. An improvement in the analytical predictions can be achieved if the load distribution is allowed to be changed during loading sequence, based on uniform end-shortening conditions.

References

1. Wagner,"Ebene blechwandtrager sehr dummen stegblech", Flugtechnik und motorluftschiflahrt, Bd.20 1929.

2. Koiter, W., T., "On the stability of elastic equilibrium" (In Dutch), thesis, Delft H. J. Paris, Amsterdam, 1945. English translation, Air-force Flight Dyn. Lab. Tech. Rep. AFFDL-TR-70-25, WPAFB, 1976.

3. Ashton, J. E. and Waddoups, M. E.,"Analysis of anisotropic plates". Journal Of Composite Materials. 3(January 1969) 148-165.

4. Ashton, J. E. and Waddoups, M. E. "Analysis of anisotropic plates II. ". Journal Of Composite Materials. 3(July 1969) 470-479.

5. Ashton,J. E. "Anisotropic plate analysis- boundary condition". Journal Of Composite Materials. 4(April 1970) 163-167.

6. Ashton, J. E. and Love, T. S.]Experimental study of the stability of composite plates". Journal Of Composite Materials. 3(April 1969)230-242.

7. Agarwal, B. L. "Post-buckling behavior of composite shear webs". AIAA Journal, Vol. 19 No. 7. 933-939, 1981.

8. Kudva, N. j. and Agrawal, B. I. "Post-buckling analysis of stiffened composite shear panels-Theoretical analysis and comparisons with experiments". Proceeding of the 102nd ASME Winter Annual Meeting, November 1981.

9. Starnes, J. H. Jr and Rouse, M. "Post-buckling and failure characteristics of selected flat rectangular Graphite-Epoxy plates loaded in compression". Proceedings of the AIAA/ASME/ ASCE/AHS 22nd SDM conference. Atlanta Georgia. April 1981.

10. Starnes, J. H. Jr and Rouse. M. "Post-buckling behavior of selected flat stiffened Graphite-Epoxy panels loaded in compression" .Proceeding of the AIAA/ASME/ASCE/AHS 23rd SDM Conference. Lake Tahoe, Nevada. May 1982.

11. Chia, C. , Y. "Nonlinear analysis of plates", McGraw-Hill, New York, 1980.

12. Leissa, A. , w. "Analysis of laminated composite plates and shell panels" , AFWAL-TR-85-3069, AF Wright Patterson Aeronautical lab. Jan. 1985.

13. Dickson, J. N. ,Cole, R. ,T. , and Wang, J. ,T. , S., "Design of stiffened composite panel in the post-buckling range", Fibrous Composite In Structural Design, 313-327, 1980.

14. Brooks, W. , G. "The design and construction of a post-buckling carbon fibre wing box structure" , ICAS-86-4.2.1.

15. Weller, T. , Kollet, M. , Libaii, A. , and Singer, J. "Durability under repeated buckling of stiffened shear panels", 14th ICAS Conference, Toulouse, France, 932-942, September 1984.

16. Segal, A. , Siton, G. , Weller, T. , " Durability of Graphite-Epoxy stiffened panels under cycling post-buckling compression loading" Proc. ICCM VI/ECCM, London, July 87.

17. Renieri, M., P., Garrett, R., A., "Investigation of the local buckling, postbuckling and crippling behavior of graphite/epoxy short thin-walled compression members", MecDonnell Aircraft Company, MDC A7091, July, 1981.

18. Sheinman, I., Frostig, Y., "Post-buckling analysis of stiffened laminated panels", to be published in the Journal of Applied Mechanics.

19. Sheinman, I., Frostig, Y., "Bifurcation Buckling Analysis of Stiffened Composite Laminated panels", to be published in the Josef Singer Anniversary Volume, Oct. 1988.